Identification of Ablation Sites in Atrial Flutter by Causal Method

Miguel Rodrigo[1], Alejandro Liberos[1], Andreu M Climent[1,2], Maria S Guillem[1]

[1]Universitat Politècnica de València, València, Spain
[2]Hospital General Universitario Gregorio Marañón, Madrid, Spain

Abstract

A 3D atrial model was used to simulate the electrical activity of four different flutter propagation patterns: typical flutter, reverse typical flutter, superior vena cava flutter and inferior vena cava flutter. In this study we propose the use of the causal method to analyse the intracardiac atrial signal in order to automatically obtain the optimal target site for ablation.

The causal method summarizes the electrical activity recorded by the electrograms in a single map, called recurrence map (RM). Three main regions can be identified in this map: (1) atrial tissue that does not belong to the re-entrant circuit, (2) atrial tissue belonging to the re-entrant circuit and (3) the thinnest path in the re-entrant circuit, with RM values of 0.03 ± 0.04, 0.41 ± 0.16 and 0.95 ± 0.05, respectively. The region with highest RM values corresponds to the optimal site for the ablation therapy.

The results obtained with atrial models during flutter suggest that the proposed method allows the identification of target sites for ablation in patients with atrial flutter. This method may be useful in clinical practice to obtain atrial propagation patterns from patients with atypical atrial flutter circuits and identify the best target regions for ablation.

1. Introduction

Atrial flutter (AFL) is a supraventricular arrhythmia provoked by a macro-reentry of the electrical wave around a physiologic obstacle. Depending on the obstacle that surrounds the macro-reentry, AFL is classified into two categories: flutters with a re-entry around the tricuspid valve (TV) are known as typical flutter, and those in which the TV is not involved are atypical [1]. Although AFL is not a mortal arrhythmia, it affects life quality due to the higher ventricular activation rate [2].

Ablation therapy provides satisfactory outcomes in patients with typical flutter. This intervention consists on breaking the re-entrant circuit, normally in its thinnest path [3]. In typical AFL this narrowest path usually is the cavotricuspid isthmus. However, in patients with atypical AFL it is necessary to identify the re-entrant circuit provoking the arrhythmia and to find the best site for the ablation. Identification of the macro-reentrant circuit is sometimes complicated using either electrocardiographic signals or intracavitary recordings. The location of target sites in atypical AFL normally is performed by using isochronal maps, although in some cases these maps are complex and thus the identification of the target site for ablation is complex. For this reason, success rates are lower in atypical flutter than in typical flutter.

This work makes use of models of atrial electrical activity to study the effectiveness of the causal method on locating the macro-reentrant path and its thinnest area. This tool can be useful for helping in ablation procedures.

2. Data base

Signals used in causal analysis were obtained by computing electrograms over atrial electrical activity simulations. Macro-reentrant activity of a 3D right atrial (RA) model with 101.214 nodes [4] was simulated using the formulation for atrial ionic currents proposed by Courtemanche [5]. For the resolution of the differential equations system, it was used the Runge-Kutta integration method with an adaptive temporal step based on a graphic processors unit [6].

Four AFL patterns were simulated: (1) typical counterclockwise flutter (Fig. 1.A); (2) typical clockwise flutter (Fig. 2.A); (2) superior vena cava (SVC) flutter (Fig. 3.A); and (4) inferior vena cava (IVC) flutter (Fig. 4.A).

From each mathematical simulation, a uniform mesh of 150 pseudo-unipolar electrograms (EGM, 1 mm from myocardial wall) was calculated under the assumption of a homogenous, unbounded and quasi-static medium by using the following expression:

$$V_{\vec{r}} = \sum_{\vec{r}} \left(\frac{\vec{r}}{r^3}\right) \cdot \vec{\nabla} V_m \qquad (1)$$

where $\vec{r}$ is the distance vector between the measuring point and a point in the tissue domain (r is the distance scalar), and $\vec{\nabla}$ denotes the gradient operator. All signals were re-sampled at sampling frequency of 1 kHz.

3. Methods

Causal relations were searched between *N=150* neighboring signals placed on a uniform mesh in the RA. Signals were divided into K_n overlapping segments of length equal to the inverse of the dominant frequency.

Each pair of simultaneous EGM observations $x_i(t)$ and $x_j(t)$ obtained from neighboring nodes was assumed to be represented by an autoregressive model (ARM):

$$x_i(t) = \sum_{\tau=t_{min}}^{t_{max}} a_\tau \cdot x_j(t-\tau) + \varepsilon_{ij}(t) \quad (2)$$

where a_τ were the ARM coefficients, and $\varepsilon_{ij}(t)$ was the error in the prediction of x_i from x_j, which can be assumed to be a white noise process characterized by its variance $\sigma^2_{\varepsilon_{ij}}$. The order of the ARM model was given by the size of the search window t_{max}-t_{min}. ARM coefficients were estimated by using the least-squares method.

The Influence Ratio (IR) matrix was obtained, computed for a given pair of signals (i,j) as the ratio between variances of the error of ARM models for the source signal ($\sigma^2_{\varepsilon_{ij}}$) and for itself ($\sigma^2_{\varepsilon_{ii}}$):

$$\mathrm{IR}_{ij} = \frac{\sigma^2_{\varepsilon_{ii}}}{\sigma^2_{\varepsilon_{ij}}} \quad (3)$$

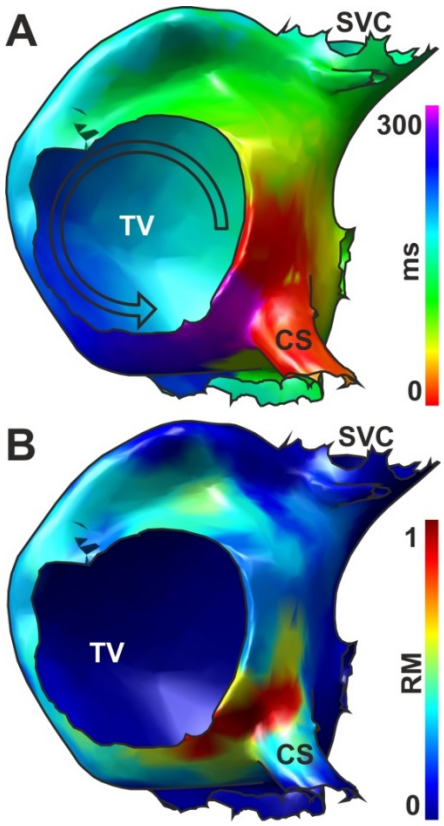

Figure 1. Typical counterclockwise flutter: (A) isochronal map of the RA, the arrow marks the rotation direction. (B) Recurrence map of the RA. SVC: superior vena cava. TV: tricuspid valve. CS: coronary sinus.

Values for IR were measured for each K_n overlapping time interval ($\mathrm{IR}_{ij,k}$). Finally, the influence of signal x_j in signal x_i was summarized by normalizing the IR matrix:

$$\mathrm{IRN}_{ij} = \frac{\frac{1}{K_n}\sum_{k=1}^{K_n} IR_{ij,k}}{\frac{1}{K_n}\sum_{k=1}^{K_n}\sum_{i=1}^{N} IR_{ij,k}} \quad (4)$$

The Recurrence Map (RM) was constructed by assigning values between 0 and 1 to each node according to the probability that the electrical signal comes from that node (i.e. 1 in for source points, 0 for sink points). These probability values (P) were computed by using the following expression:

$$P = M^{\infty} \times P_0; \quad (5)$$

where M^{∞} was the permanent regime value of IRN matrix and P_0 was the initial probability distribution where $P_{0i} = 1/N$. M^{∞} was iteratively computed as follows:

$$\mathrm{M}^t = \mathrm{M}^{t-1} \times \mathrm{M}^{t-1}, \quad \mathrm{M}^0 = \mathrm{IRN} \quad (6)$$

$$\xi = \max(\mathrm{M}^t - \mathrm{M}^{t-1}) \quad (7)$$

where M^{∞} was reached when ξ was below a threshold.

4. Results

First atrial flutter analysed was typical counterclockwise flutter, whose isochronal map is shown in Figure 1.A. As it can be observed, the electrical propagation turns around TV. Causal method applied to the electrograms obtained on the RA provided the RM observed in Figure 1.B. This map contains values close to zero at atrial zones that not belong to the macro re-entrant circuit, and values between 0.2 and 0.7 at the surroundings of the TV. The narrowest zone of this re-entrant path, between the TV and coronary sinus (CS), is marked with the highest values of the RM map.

The isochronal map of the typical clockwise flutter is depicted in Figure 2.A. In this case there is again a macro-reentry around the TV, as in the previous case but with opposite propagation direction. The RM (Fig. 2.B) marks the pathway around the TV with values between 0.4 and 0.7, and the thinnest zone, between the TV and the CS too, is marked with values close to 1.

Third AFL analysed was a superior vena cava flutter (Fig. 3.A), in which there is a re-entry around the superior vena cava. In this case, the RM shows values between 0.2 and 0.8 in the surroundings of the SVC (Fig. 3.B). The narrowest path of the re-entry, placed between this vena cava and the Bachman's bundle, exhibits RM values higher than 0.9.

In our last simulation there is a macro-reentry around the inferior vena cava (Fig. 4.A). This AFL is provoked after ablation of the atrial tissue between TV and CS (marked in black in Fig. 4.A) in order to terminate a

typical AFL. The re-entrant circuit around the IVC shows RM values between 0.4 and 0.8 (Fig. 5.B). The thinnest path, in this case between IVC and the lesion around the CS, depicts values close to 1.

Results obtained for all simulations are summarized in Figure 5. In all four cases, RM values obtained at the location of the re-entrant circuit were higher than 0.2, and the narrowest path of the circuit presented values higher to 0.9. Statistical significance ($p < 0.01$) was observed between the RM values from the three areas in all simulations.

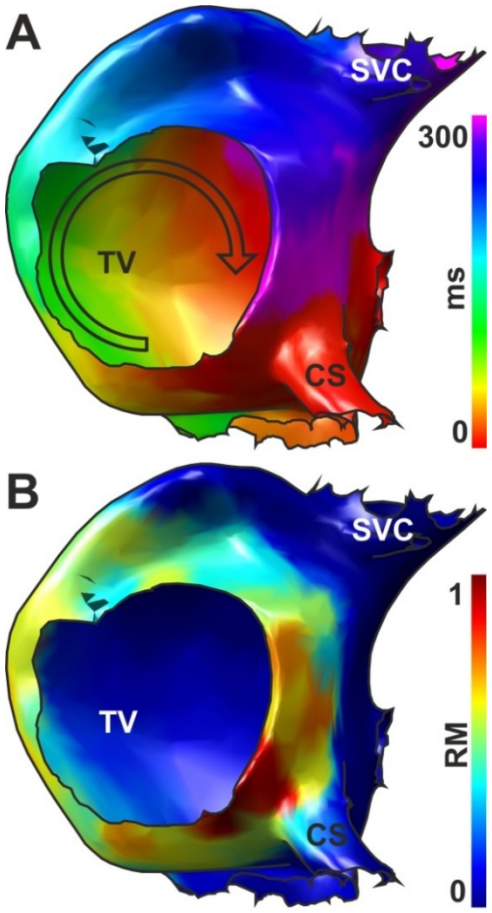

Figure 2. Typical clockwise flutter: (A) isochronal map of the RA, the arrow marks the rotation direction. (B) Recurrence map of the RA. SVC: superior vena cava. TV: tricuspid valve. CS: coronary sinus.

5. Discussion

This computational study describes a novel methodology based on causal theory that allows to identify the macro-reentrant circuit present during AFL and its narrowest path, target for ablation procedures. Its applicability has been proved on four atrial macro-reentrant propagation patterns simulated with a 3D mathematical model of atrial electrical activity. Results of causal analysis of intracardiac electrical signals are presented in a single map where the reentrant circuit and its thinnest past can be easily located.

Although AFL can be effectively diagnosed with non-invasive methods such as electrocardiogram, identification of the macro-reentrant path involved in the macroreentry is not easy, especially in atypical and post-ablation AFL [3]. In cases at which the propagation pattern during AFL cannot be determined from the standard electrocardiogram, the electrophysiologist makes use of isochronal maps computed from intracardiac atrial signals to identify both the re-entrant path and the best site for ablation. However, isochronal maps sometimes are hard interpret and, therefore, the outcome of ablation therapies depend on clinical experience.

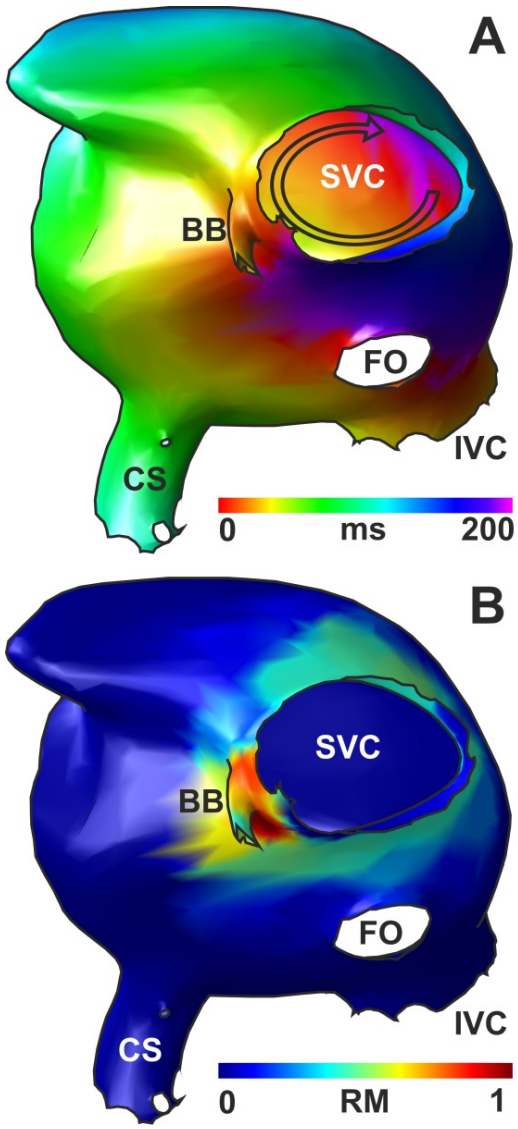

Figure 3. Superior vena cava flutter: (A) isochronal map of the RA, the arrow marks the rotation direction. (B) Recurrence map of the RA. SVC: superior vena cava. FO: fossa ovalis. CS: coronary sinus. IVC: inferior vena cava. BB: Bachman's bundle.

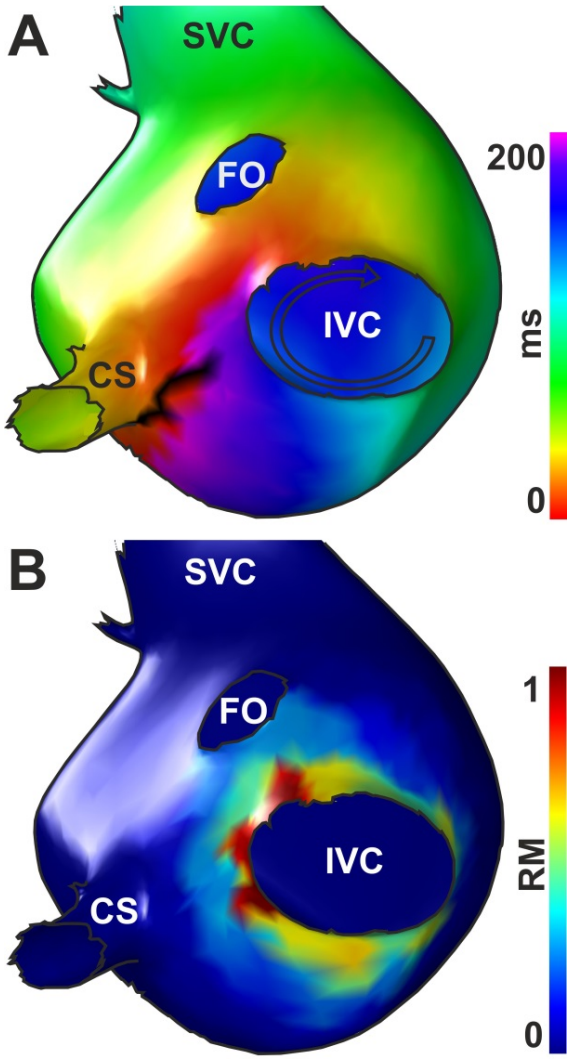

Figure 4. Inferior vena cava flutter: (A) isochronal map of the RA, the arrow marks the rotation direction. Lesion is marked in black. (B) Recurrence map of the RA. SVC: superior vena cava. FO: fossa ovalis. CS: coronary sinus. IVC: inferior vena cava.

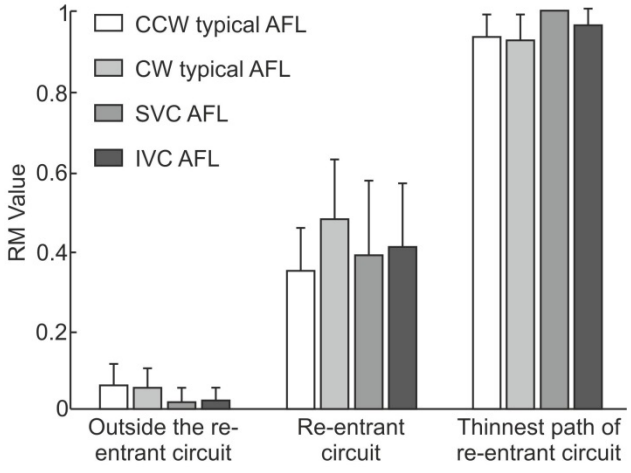

Figure 5. Values from RM for the four simulated flutters.

Causality-based analysis has been used to identify he propagation pattern which governs the electrical activity in the myocardium [7-8]. This method has been proved useful to obtain the electrical sources of atrial activity during arrhythmias. In case of AFL, causal method allows the clinician to recognize in an easy and unequivocal way the electrical path involved in the the macro-reentry and the ablation target. Validation of the presented methodology in mathematical models of AFL aims us to evaluate the feasibility of the causal method in patients as the next step. Recurrence maps obtained with causal analysis may be useful to characterize AFL propagation patterns on each individual patient and may serve as guidance for ablation procedures.

Acknowledgements

This work was partially supported by Generalitat Valenciana (GV/2012/039) and by Universitat Politècnica de València through its research initiative program.

References

[1] Saoudi N, Cosio F, Waldo A, Chen S, Iesaka Y, Lesh M, Saksena S, Salerno J, Schoels W. A classification of atrial flutter and regular atrial tachycardia according to electrophysiological mechanisms and anatomical bases - A statement from a Joint Expert Group from the Working Group of Arrhythmias of the European Society of Cardiology and the North American Society of Pacing and electrophysiology. Eur. Heart J 2001; 22:1162-82.

[2] Garcia-Cosio F, Pastor Fuentes A, Nunez Angulo A. Clinical approach to atrial tachycardia and atrial flutter from an understanding of the mechanisms: electrophysiology based on anatomy. Rev Esp Cardiol 2012; 65:363-75.

[3] Morady F. Drug therapy - Radio-frequency ablation as treatment for cardiac arrhythmias. N Engl J Med 1999; 340:534-44.

[4] Harrild DM, Henriquez CS. A computer model of normal conduction in the human atria. Circ Res 2000; 87:E25-36.

[5] Courtemanche M, Ramirez RJ, Nattel S. Ionic mechanisms underlying human atrial action potential properties: insights from a mathematical model. Am J Physiol 1998;275:301-21

[6] García VM, Liberos A, Climent AM, Vidal A, Millet J, González A. An adaptative step size GPU ODE solver for simulating the electric cardiac activity. Computers in Cardiology 2011:233-6.

[7] Rodrigo M, Guillem MS, Liberos A, et al. Identification of fibrillatory sources by measuring causal relationships. Computing in Cardiology 2012;39:705-708.

[8] Richter U, Faes L, Cristoforetti A, et al. A novel approach to propagation pattern analysis in intracardiac atrial fibrillation signals. Ann Biomed Eng 2011;39:310-23.

Address for correspondence.
M. Rodrigo
BioITACA, Universitat Politècnica de València
mirodbor@teleco.upv.es